I3D: TRANSFORMER ARCHITECTURES WITH INPUT-DEPENDENT DYNAMIC DEPTH FOR SPEECH RECOGNITION

Yifan Peng¹, Jaesong Lee², Shinji Watanabe¹

¹Carnegie Mellon University ²NAVER Corporation

ABSTRACT

Transformer-based end-to-end speech recognition has achieved great success. However, the large footprint and computational overhead make it difficult to deploy these models in some real-world applications. Model compression techniques can reduce the model size and speed up inference, but the compressed model has a fixed architecture which might be suboptimal. We propose a novel Transformer encoder with Input-Dependent Dynamic Depth (I3D) to achieve strong performance-efficiency trade-offs. With a similar number of layers at inference time, I3D-based models outperform the vanilla Transformer and the static pruned model via iterative layer pruning. We also present interesting analysis on the gate probabilities and the input-dependency, which helps us better understand deep encoders.

Index Terms— Dynamic depth, transformer, speech recognition

1. INTRODUCTION

Recently, end-to-end automatic speech recognition (ASR) has gained popularity. Typical frameworks include Connectionist Temporal Classification (CTC) [1], Attention-based Encoder-Decoder (AED) [2–4], and Recurrent Neural Network Transducer (RNN-T) [5]. Many types of networks can be used as encoders in these frameworks, such as Convolutional Neural Networks (CNNs), RNNs, Transformers [6] and their combinations [7–9]. Transformers have achieved great success in various benchmarks [10]. However, they usually contain many cascaded blocks and thus have high computation, which hinders deployment in some real-world applications with limited resource. To reduce computation and speed up inference, researchers have investigated different approaches.

A popular method is to compress a large pre-trained model using distillation [11–13], pruning [14–16], and quantization [15]. However, the compressed model has a fixed architecture for all types of inputs, which might be suboptimal. For example, this fixed model may be too expensive for very easy utterances but insufficient for difficult ones. To better trade off performance and computation, prior studies have explored dynamic models [17], which can adapt their architectures to different inputs. Dynamic models have shown to be effective in computer vision [18-23], which are mainly based on CNNs. For speech processing, [24] trains two RNN encoders of different sizes and dynamically switches between them guided by keyword spotting. [25] proposes a dynamic encoder transducer based on laver dropout and collaborative learning. [26] adopts two RNN encoders to tackle close-talk and far-talk speech. [27] also designs two RNN encoders that are compressed to different degrees and switches between them on a frame-by-frame basis. [28] extends this idea to Transformer-transducers and considers more flexible subnetworks, but it continues to focus on streaming ASR and the architecture is

still determined on a frame-by-frame basis, which requires a special design for the fined-grained key and query operations in self-attention. For nonstreaming (or chunk-based streaming) ASR, the frame-level prediction may be expensive and suboptimal, as it only captures frame-level local features.

We propose a Transformer encoder with Input-Dependent Dynamic Depth (I3D) for end-to-end ASR. Instead of using carefully designed fine-grained operations within submodules like attention, I3D predicts whether to skip an entire self-attention block or an entire feed-forward network through a series of local gate predictors or a single global gate predictor. The prediction is made at the utterance level (or chunk level if extended to streaming cases), which is easier to implement and reduces additional cost. It also captures global statistics of the input. As analyzed in Sec. 3.4, the length of an utterance affects the inference architecture. Some blocks may be useful for longer inputs. Results show that I3D models consistently outperform Transformers trained from scratch and the static pruned models via iterative layer pruning [29], when using a similar number of layers for inference. We also perform interesting analysis on predicted gate probabilities and input-dependency, which helps us better understand the behavior of deep encoders.

2. METHOD

2.1. Transformer encoder

A Transformer [6] encoder layer contains a multi-head self-attention (MHA) module and a feed-forward network (FFN), which are combined sequentially. The function of the *l*-th layer is as follows:

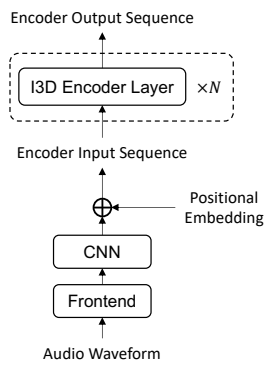
$$\mathbf{Y}^{(l)} = \mathbf{X}^{(l-1)} + MHA^{(l)}(\mathbf{X}^{(l-1)}), \tag{1}$$

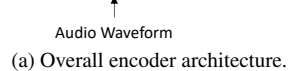
$$\mathbf{X}^{(l)} = \mathbf{Y}^{(l)} + \text{FFN}^{(l)}(\mathbf{Y}^{(l)}), \tag{2}$$

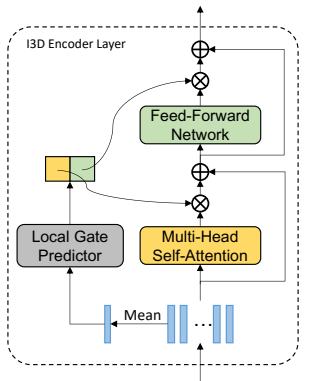
where $\mathbf{X}^{(l)}$ is the output of the l-th Transformer layer and $\mathbf{X}^{(l-1)}$ is thus the input to the l-th layer. $\mathbf{Y}^{(l)}$ is the output of the MHA at the l-th layer, which is also the input of the FFN at the l-th layer. These sequences all have a length of T and a feature size of d.

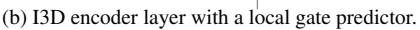
2.2. Overall architecture of I3D encoders

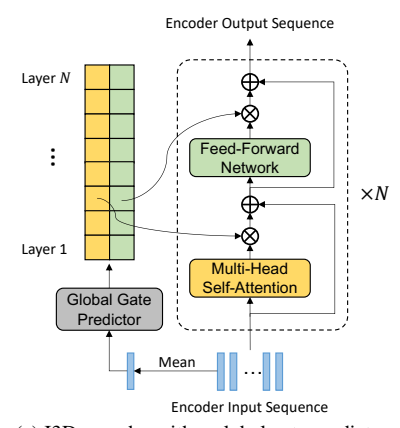
Fig. 1a shows the overall architecture of I3D encoders. A waveform is first converted to a feature sequence by a frontend, and further processed and downsampled by a CNN, after which positional embeddings are added. Later, the sequence is processed by a stack of N I3D encoder layers to produce high-level features. This overall design follows that of Transformer. However, Transformer always uses a fixed architecture regardless of the input. Our I3D selects different combinations of MHA and FFN depending on the input utterance. To determine whether a module should be executed or skipped, a $bi-nary\ gate$ is introduced for each MHA or FFN module. The function











(c) I3D encoder with a global gate predictor.

Fig. 1: Architectures of our proposed I3D encoders.

of the l-th layer (see Eqs. (1) and (2) for the vanilla Transformer) now becomes:

$$\mathbf{Y}^{(l)} = \mathbf{X}^{(l-1)} + g_{\text{MHA}}^{(l)} \cdot \text{MHA}^{(l)}(\mathbf{X}^{(l-1)}), \tag{3}$$

$$\mathbf{X}^{(l)} = \mathbf{Y}^{(l)} + g_{\text{FFN}}^{(l)} \cdot \text{FFN}^{(l)} (\mathbf{Y}^{(l)}), \tag{4}$$

where $g_{\text{MHA}}^{(l)},g_{\text{FFN}}^{(l)}\in\{0,1\}$ are input-dependent gates. If a gate is predicted to be 0, then the corresponding module will be skipped, which effectively reduces computation. The total training loss is:

$$\mathcal{L}_{total} = \mathcal{L}_{ASR} + \lambda \cdot \mathcal{L}_{utility}, \tag{5}$$

$$\mathcal{L}_{\text{utility}} = \frac{1}{2N} \sum_{l=1}^{N} \left(g_{\text{MHA}}^{(l)} + g_{\text{FFN}}^{(l)} \right), \tag{6}$$

where \mathcal{L}_{ASR} is the standard ASR loss and $\mathcal{L}_{utility}$ is a regularization loss measuring the utility rate of all MHA and FFN modules. $\lambda > 0$ is a hyper-parameter to trade off the recognition accuracy and computational cost. 1 Note that the utility loss in Eq. (6) is defined for an individual utterance so the utterance index is omitted. In practice, a mini-batch is used and the loss is averaged over utterances.

A major issue with this training objective is that binary gates are not differentiable. To solve this problem, we apply the Gumbel-Softmax [30, 31] trick, which allows drawing hard (or soft) samples from a discrete distribution. Consider a discrete random variable Z with probabilities $P(Z=k) \propto \alpha_k$ for any $k=1,\ldots,K$. To draw a sample from this distribution, we can first draw K i.i.d. samples $\{g_k\}_{k=1}^K$ from the standard Gumbel distribution and then select the index with the largest perturbed log probability:

$$z = \underset{k \in \{1, \dots, K\}}{\operatorname{arg max}} \log \alpha_k + g_k. \tag{7}$$

The argmax is not differentiable, which can be relaxed to the softmax. It is known that any sample from a discrete distribution can be denoted as a one-hot vector, where the index of the only non-zero entry is the desired sample. With this vector-based notation, we can draw a soft sample as follows:

$$\mathbf{z} = \operatorname{softmax} \left((\log \alpha + \mathbf{g}) / \tau \right),$$
 (8)

where $\alpha = (\alpha_1, \dots, \alpha_K)$, $\mathbf{g} = (g_1, \dots, g_K)$, and τ is a temperature constant. Eq. (8) is an approximation of the original sampling process, but it is differentiable w.r.t. α and thus suitable for gradientbased optimization. As $\tau \to 0$, the approximation becomes closer to the discrete version. We use $\tau=1$ in our experiments.

For the *l*-th MHA, a discrete probability distribution $\mathbf{p}_{\text{MHA}}^{(l)} \in \mathbb{R}^2$ over two possible gate values (0 and 1) is predicted, where 0 means skipping this module and 1 means executing it. Then, a soft sample is drawn from this discrete distribution using Eq. (8), which is used as the gate in Eq. (3) during training. Similarly, for the l-th FFN, a distribution $\mathbf{p}_{\text{FFN}}^{(l)} \in \mathbb{R}^2$ is predicted, from which a soft gate is drawn and used in Eq. (4). The gate distributions are generated by a gate predictor based on the input features, as defined in Sec. 2.3.

2.3. Local and global gate predictors

We propose two types of gate predictors, namely the local gate predictor and global gate predictor. We employ a multi-layer perceptron (MLP) with a single hidden layer of size 32 in all experiments, which has little computational overhead.

The local gate predictor (LocalGP or LGP) is associated with a specific I3D encoder layer, as illustrated in Fig. 1b. Every layer has its own gate predictor whose parameters are independent. Consider the l-th encoder layer with an input sequence $\mathbf{X}^{(l-1)} \in \mathbb{R}^{T \times d}$. This sequence is first converted to a d-dimensional vector $\mathbf{x}^{(l-1)} \in \mathbb{R}^d$ through average pooling along the time dimension. Then, this pooled vector is transformed to two 2-dimensional probability vectors for the MHA gate and the FFN gate, respectively:

$$\mathbf{p}_{\mathsf{MHA}}^{(l)}, \mathbf{p}_{\mathsf{EEN}}^{(l)} = \mathsf{LGP}^{(l)}(\mathbf{x}^{(l-1)}), \tag{9}$$

where $\mathbf{p}_{\text{MHA}}^{(l)}, \mathbf{p}_{\text{FFN}}^{(l)} \in \mathbb{R}^2$ are introduced in Sec. 2.2, and LGP^(l) is the local gate predictor at the l-th layer. With this formulation, the decision of executing or skipping any MHA or FFN module depends on the input to the current layer, which further depends on the decision made at the previous layer. Hence, the decisions are made sequentially from lower to upper layers. During inference, a fixed threshold $\beta \in [0, 1]$ is utilized to produce a binary gate for every module:

$$g_{\text{MHA}}^{(l)} = 1 \text{ if } (\mathbf{p}_{\text{MHA}}^{(l)})_1 > \beta \text{ else } 0,$$
 (10)

$$g_{\text{FFN}}^{(l)} = 1 \text{ if } (\mathbf{p}_{\text{FFN}}^{(l)})_1 > \beta \text{ else } 0,$$
 (11)

where $(\mathbf{p}_{\text{MHA}}^{(l)})_1$ is the probability of executing the MHA and $(\mathbf{p}_{\text{FFN}}^{(l)})_1$ is the probability of executing the FFN. We use $\beta = 0.5$ by default, but it is also possible to adjust the inference cost by changing β .

¹Our method can be extended to consider different costs of MHA and FFN. In Eq. (6), we can use a weighted average of the two types of gates, where the weights depend on their computational costs. Then, the training will minimize the overall computation instead of simply the number of layers.

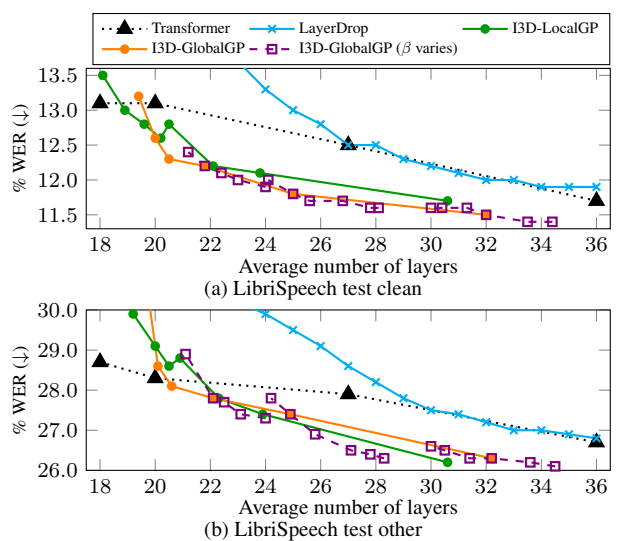


Fig. 2: Word error rates (%) of $\tilde{\mathbf{CTC}}$ -based models vs. average number of layers used for inference on **LibriSpeech** test sets. β is the threshold for generating binary gates as defined in Eqs. (10) (11).

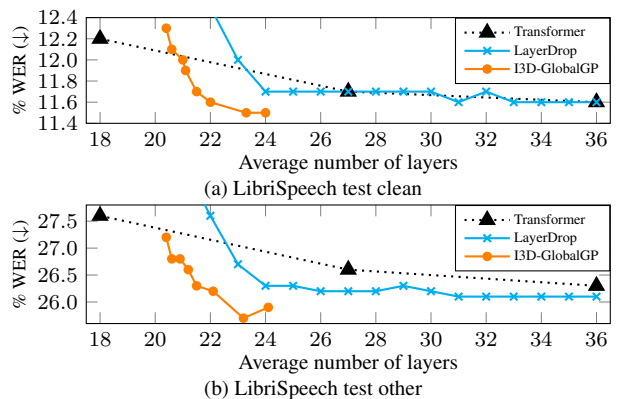


Fig. 3: Word error rates (%) of InterCTC-based models vs. average number of layers used for inference on LibriSpeech test sets.

The global gate predictor (GlobalGP or GGP), on the other hand, is defined for an entire I3D encoder, as shown in Fig. 1c. It predicts the gate distributions for all layers based on the encoder's input, which is also the input to the first layer: $\mathbf{X} = \mathbf{X}^{(0)} \in \mathbb{R}^{T \times d}$. In particular, the sequence is transformed to a single vector $\mathbf{x} = \mathbf{x}^{(0)} \in \mathbb{R}^d$ by average pooling. Then, it is mapped to two sets of probability distributions for all N MHA and FFN gates, respectively:

$$\{\mathbf{p}_{\text{MHA}}^{(l)}\}_{l=1}^{N}, \{\mathbf{p}_{\text{FFN}}^{(l)}\}_{l=1}^{N} = \text{GGP}(\mathbf{x}),$$
 (12)

where $\mathbf{p}_{\text{MHA}}^{(l)}, \mathbf{p}_{\text{FFN}}^{(l)} \in \mathbb{R}^2$ are the gate probability distributions at the l-th layer, and the I3D encoder has N layers in total. Here, the decisions of executing or skipping modules are made immediately after seeing the encoder's input, which has lower computational overhead than LocalGP and allows for more flexible control over the inference architecture. During inference, we can still use a fixed threshold $\beta \in [0,1]$ to generate binary gates as in Eqs. (10) and (11).

3. EXPERIMENTS

3.1. Experimental setup

We use PyTorch [32] and follow the ASR recipes in ESPnet [33] to train all models. We mainly use the CTC framework on LibriSpeech

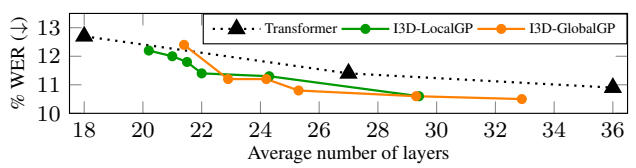


Fig. 4: Word error rates (%) of CTC-based models vs. average number of layers used for inference on the **Tedlium2** test set.

Table 1: Word error rates (%) and average number of inference layers of **AED**-based models on **LibriSpeech 100h**.

Model	dev clean		test clean	
	Ave #layers	WER (\downarrow)	Ave #layers	WER (\downarrow)
Transformer	36	7.8	36	8.0
	27	8.2	27	8.5
I3D-LGP-36	27.3	7.9	27.1	8.3
I3D-GGP-36	27.2	7.8	27.1	8.2

100h [34]. In Sec. 3.5, we also show that I3D can be applied to AED and another corpus, Tedlium2 [35]. Our I3D encoders have 36 layers in total. They are initialized with trained standard Transformers and fine-tuned with a reduced learning rate (1e-3) and various λ (usually ranging from 1 to 13) in Eq. (5) to trade off WER and computation. The fine-tuning epochs for LibriSpeech 100h and Tedlium2 are 50 and 35, respectively. We compare I3D with two baselines. First, we train standard Transformers with a reduced number of layers. Second, we train a 36-layer Transformer with LayerDrop [36, 37] or Intermediate CTC (InterCTC) [38] and perform iterative layer pruning [29] using the validation set to get a variety of models with smaller and fixed architectures. This baseline is denoted as "LayerDrop" in Figs. 2 and 3. We can compare I3D, whose layers are dynamically reduced based on the input, against the static pruned models.

3.2. Main results

Fig. 2 compares our I3D models with two baselines. We train I3D-CTC models with different λ in Eq. (5) to adjust the operating point. We calculate the number of layers as the average of the number of MHA blocks and the number of FFN blocks. Both I3D-LocalGP and I3D-GlobalGP outperform the standard Transformer and the pruned version using iterative layer pruning [29]. We can reduce the average number of layers to around 20 while still matching the Transformer trained from scratch. LocalGP achieves similar performance as GlobalGP, but GlobalGP has only one gate predictor, which can be more efficient for inference. The reason why LocalGP is not better than GlobalGP may be that LocalGP decides whether to execute or skip a block based on the current layer's input, which depends on decisions at previous layers. This sequential procedure can lead to more severe error propagation. We also show that it is possible to adjust the computational cost of a trained I3D model by changing β (see Eqs. (10) (11)) at inference time. Three I3D-GlobalGP models are decoded with different β . As β decreases, more blocks are used, and the WER is usually improved.

Fig. 3 shows the results using InterCTC [38]. The WERs are lower than those in Fig. 2, thanks to the auxiliary CTC loss which regularizes training. Again, I3D is consistently better than the Transformer trained from scratch and the pruned model.

3.3. Analysis of gate distributions

Fig. 5 shows the mean and standard deviation (std) of the gate probabilities generated by an I3D-GlobalGP model using CTC on Lib-

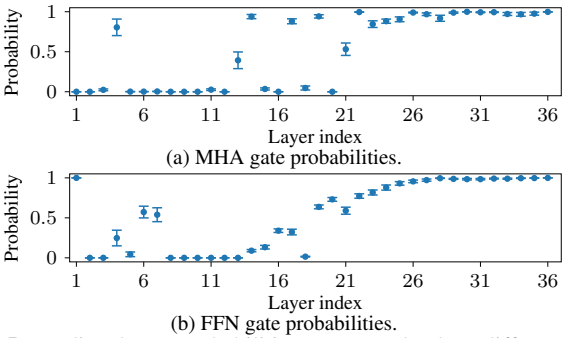


Fig. 5: Predicted gate probabilities (mean and std) at different layers of an I3D-GlobalGP model on LibriSpeech test other. A higher probability means the layer is more likely to be executed.

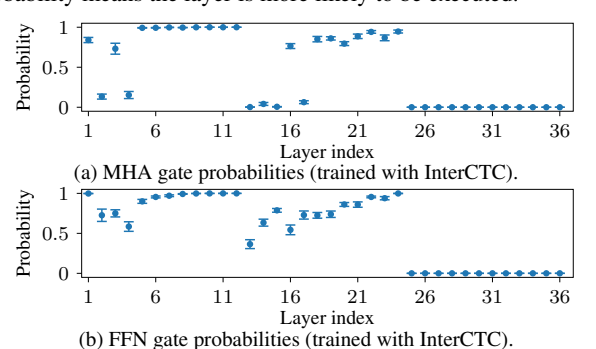


Fig. 6: Predicted gate probabilities (mean and std) at different layers of an I3D-GlobalGP model with InterCTC on LibriSpeech test other. A higher probability means the layer is more likely to be executed.

riSpeech test-other. Most layers have a stable probability. Several layers have larger variations depending on the input. For both MHA and FFN, upper layers are executed with high probabilities while lower layers tend to be skipped, which is consistent with [28].

We also show the gate probabilities from an I3D-GlobalGP model trained with InterCTC [38] in Fig. 6. Interestingly, the overall trend is very different from Fig. 5. Now, the upper layers are almost skipped while the lower layers are executed with very high probabilities, indicating that lower layers of this encoder can learn powerful representations for the ASR task. This is probably because auxiliary CTC losses inserted at intermediate layers can facilitate the gradient propagation to lower parts of a deep encoder, which effectively improves its capacity and also the final performance.

We believe this gate analysis can provide a way to interpret the layer-wise behavior of deep networks.

3.4. Analysis of input-dependency

It has been shown that our I3D models can dynamically adjust the encoder depth based on the characteristics of an input utterance, which achieves strong performance even with reduced computation. But it is unclear which features are important for the gate predictor to determine the modules used during inference. We have found that the speech length generally affects the inference architecture. Fig. 7 shows the speech length distributions categorized by the number of MHA or FFN blocks used by an I3D-GlobalGP model during inference. We observe that utterances using more blocks tend to be longer. This is probably because longer utterances contain more complex information and longer-range dependency among frames, which require more blocks (especially MHA) to process.

We also considered two other factors that may affect the infer-

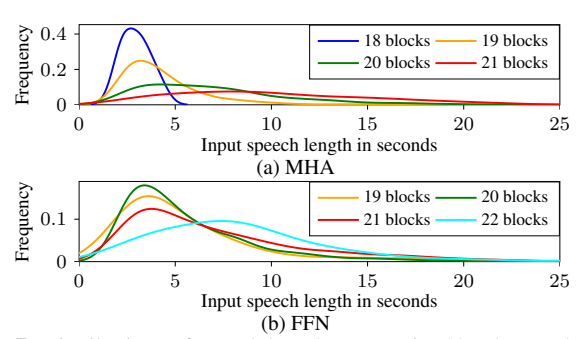


Fig. 7: Distributions of speech lengths categorized by the number of MHA or FFN blocks used for inference. This is an I3D-GlobalGP model evaluated on LibriSpeech test other. Utterances using more blocks tend to be longer.

ence architecture, namely the difficulty of utterances measured by WERs, and the audio quality measured by DNSMOS scores [39]. However, in general, we didn't observe a clear relationship between these metrics and the number of layers used for inference.

3.5. Generalizability

We demonstrate that the proposed I3D encoders can be directly applied to other datasets and ASR frameworks. Fig. 4 shows the results of CTC-based models on Tedlium2. Our I3D models consistently achieve lower WERs than the standard Transformer with similar or even fewer layers during inference. ² We further apply I3D to the attention-based encoder-decoder (AED) framework. Only the encoder is changed while the decoder is still a standard Transformer decoder. Table 1 presents the results on LibriSpeech 100h. With around 27 layers on average during inference, our I3D models outperform the 27-layer Transformer trained from scratch on both dev clean and test clean sets. The I3D with a global gate predictor is slightly better than that with a local gate predictor.

4. CONCLUSION

In this work, we propose I3D, a Transformer-based encoder which dynamically adjusts its depth based on the characteristics of input utterances to trade off performance and efficiency. We design two types of gate predictors and show that I3D-based models consistently outperform the vanilla Transformer trained from scratch and the static pruned model. I3D can be applied to various end-to-end ASR frameworks and corpora. We also present interesting analysis on the predicted gate probabilities and the input-dependency to better interpret the behavior of deep encoders and the effect of intermediate loss regularization techniques. In the future, we plan to apply this method to large pre-trained models. We will explore only fine-tuning gate predictors to significantly reduce training cost.

5. ACKNOWLEDGEMENTS

This work used Bridges2 at PSC and Delta at NCSA through allocation CIS210014 from the Advanced Cyberinfrastructure Coordination Ecosystem: Services & Support (ACCESS) program, which is supported by National Science Foundation grants #2138259, #2138286, #2138307, #2137603, and #2138296.

 $^{^2\}mbox{We}$ have also evaluated I3D on LibriSpeech 960h. Observations are consistent with LibriSpeech 100h and Tedlium2.

6. REFERENCES

- [1] A. Graves, S. Fernández, et al., "Connectionist temporal classification: labelling unsegmented sequence data with recurrent neural networks," in *Proc. ICML*, 2006.
- [2] K. Cho, B. Merrienboer, et al., "Learning phrase representations using RNN encoder-decoder for statistical machine translation," in *Proc. EMNLP*, 2014.
- [3] D. Bahdanau, K. Cho, et al., "Neural machine translation by jointly learning to align and translate," in *Proc. ICLR*, 2015.
- [4] W. Chan, N. Jaitly, et al., "Listen, attend and spell: A neural network for large vocabulary conversational speech recognition," in *Proc. ICASSP*, 2016.
- [5] A. Graves, "Sequence transduction with recurrent neural networks," *arXiv:1211.3711*, 2012.
- [6] A. Vaswani, N. Shazeer, N. Parmar, et al., "Attention is all you need," in *Proc. NeurIPS*, 2017.
- [7] A. Gulati, J. Qin, C.-C. Chiu, et al., "Conformer: Convolutionaugmented Transformer for Speech Recognition," in *Proc. Interspeech*, 2020.
- [8] Y. Peng, S. Dalmia, et al., "Branchformer: Parallel MLPattention architectures to capture local and global context for speech recognition and understanding," in *Proc. ICML*, 2022.
- [9] K. Kim, F. Wu, Y. Peng, et al., "E-branchformer: Branchformer with enhanced merging for speech recognition," arXiv:2210.00077, 2022.
- [10] S. Karita, N. Chen, T. Hayashi, et al., "A comparative study on transformer vs rnn in speech applications," in *Proc. ASRU*, 2019.
- [11] G. Hinton, O. Vinyals, J. Dean, et al., "Distilling the knowledge in a neural network," *arXiv:1503.02531*, 2015.
- [12] H. Chang, S. Yang, and H. Lee, "Distillubert: Speech representation learning by layer-wise distillation of hidden-unit bert," in *Proc. ICASSP*, 2022.
- [13] R. Wang, Q. Bai, et al., "LightHuBERT: Lightweight and Configurable Speech Representation Learning with Once-for-All Hidden-Unit BERT," in *Proc. Interspeech*, 2022.
- [14] P. Dong, S. Wang, et al., "RTMobile: Beyond Real-Time Mobile Acceleration of RNNs for Speech Recognition," in ACM/IEEE Design Automation Conference (DAC), 2020.
- [15] K. Tan and D.L. Wang, "Compressing deep neural networks for efficient speech enhancement," in *Proc. ICASSP*, 2021.
- [16] C. J. Lai, Y. Zhang, et al., "Parp: Prune, adjust and re-prune for self-supervised speech recognition," in *Proc. NeurIPS*, 2021.
- [17] Y. Han, G. Huang, S. Song, et al., "Dynamic neural networks: A survey," *IEEE Trans. Pattern Anal. Mach. Intell.*, vol. 44, no. 11, pp. 7436–7456, 2022.
- [18] E. Bengio, P. Bacon, et al., "Conditional computation in neural networks for faster models," arXiv:1511.06297, 2015.
- [19] A. Veit and S. Belongie, "Convolutional networks with adaptive inference graphs," in *Proc. ECCV*, 2018.
- [20] X. Wang, F. Yu, et al., "Skipnet: Learning dynamic routing in convolutional networks," in *Proc. ECCV*, 2018.
- [21] Z. Wu, T. Nagarajan, et al., "Blockdrop: Dynamic inference paths in residual networks," in *Proc. CVPR*, 2018.

- [22] J. Shen, Y. Wang, et al., "Fractional skipping: Towards finer-grained dynamic cnn inference," in *Proc. AAAI*, 2020.
- [23] C. Li, G. Wang, et al., "Dynamic slimmable network," in *Proc. CVPR*, 2021.
- [24] J. Macoskey, G. P. Strimel, and A. Rastrow, "Bifocal neural asr: Exploiting keyword spotting for inference optimization," in *Proc. ICASSP*, 2021.
- [25] Y. Shi, V. Nagaraja, C. Wu, et al., "Dynamic encoder transducer: a flexible solution for trading off accuracy for latency," arXiv:2104.02176, 2021.
- [26] F. Weninger, M. Gaudesi, R. Leibold, R. Gemello, and P. Zhan, "Dual-encoder architecture with encoder selection for joint close-talk and far-talk speech recognition," in *Proc. ASRU*, 2021
- [27] J. Macoskey, G. P. Strimel, J. Su, and A. Rastrow, "Amortized neural networks for low-latency speech recognition," arXiv:2108.01553, 2021.
- [28] Y. Xie, J. J. Macoskey, et al., "Compute Cost Amortized Transformer for Streaming ASR," in *Proc. Interspeech*, 2022.
- [29] J. Lee, J. Kang, and S. Watanabe, "Layer pruning on demand with intermediate CTC," in *Proc. Interspeech*, 2021.
- [30] E. Jang, S. Gu, and B. Poole, "Categorical reparameterization with gumbel-softmax," in *Proc. ICLR*, 2017.
- [31] C. J. Maddison, A. Mnih, and Y. Teh, "The concrete distribution: A continuous relaxation of discrete random variables," in *Proc. ICLR*, 2017.
- [32] A. Paszke, S. Gross, F. Massa, et al., "Pytorch: An imperative style, high-performance deep learning library," in *Proc. NeurIPS*, 2019.
- [33] S. Watanabe, T. Hori, S. Karita, et al., "ESPnet: End-to-End Speech Processing Toolkit," in *Proc. Interspeech*, 2018.
- [34] V. Panayotov, G. Chen, D. Povey, and S. Khudanpur, "Librispeech: An ASR corpus based on public domain audio books," in *Proc. ICASSP*, 2015.
- [35] A. Rousseau, P. Deléglise, Y. Esteve, et al., "Enhancing the ted-lium corpus with selected data for language modeling and more ted talks.," in *Proc. LREC*, 2014.
- [36] G. Huang, Y. Sun, Z. Liu, D. Sedra, and K. Weinberger, "Deep networks with stochastic depth," in *Proc. ECCV*, 2016.
- [37] A. Fan, E. Grave, and A. Joulin, "Reducing transformer depth on demand with structured dropout," in *Proc. ICLR*, 2020.
- [38] J. Lee and S. Watanabe, "Intermediate loss regularization for ctc-based speech recognition," in *Proc. ICASSP*, 2021.
- [39] C. K. Reddy, V. Gopal, and R. Cutler, "Dnsmos p.835: A non-intrusive perceptual objective speech quality metric to evaluate noise suppressors," in *Proc. ICASSP*, 2022.